Assessment of the Multipath Mitigation Effect of Vector Tracking in an Urban Environment

Li-Ta Hsu[1], Paul D Groves[2], Shau-Shiun Jan[1]
[1] *Department of Aeronautics and Astronautics, National Cheng Kung University, Taiwan*
[2] *Faculty of Engineering, University College London, UK*

BIOGRAPHY

Li-Ta Hsu is a Ph.D. candidate in the Department of Aeronautics and Astronautics at National Cheng Kung University (NCKU) in Taiwan. In 2012, he was a visiting Ph. D. student in the Faculty of Engineering at University College London (UCL). He has published papers on indoor positioning, GNSS signal processing and multipath mitigation. He received his B.S. degree in Aeronautics and Astronautics from National Cheng Kung University in 2007.

Dr Paul Groves is a Lecturer (academic faculty member) at UCL, where he leads a program of research into robust positioning and navigation. He joined in 2009, after 12 years of navigation systems research at DERA and QinetiQ. He is interested in all aspects of navigation and positioning, including multi-sensor integrated navigation, improving GNSS performance under challenging reception conditions, and novel positioning techniques. He is an author of about 50 technical publications, including the book *Principles of GNSS, Inertial and Multi-Sensor Integrated Navigation Systems*, now in its second edition. He is a Fellow of the Royal Institute of Navigation and an associate editor of both *Navigation: Journal of the ION* and *IEEE Transactions on Aerospace and Electronic Systems*. He holds a BA/MA and a DPhil in physics from the University of Oxford (p.groves@ucl.ac.uk).

Shau-Shiun Jan is an associate Professor of the Department of Aeronautics and Astronautics at NCKU in Taiwan. He directs the NCKU Communication and Navigation Systems Laboratory (CNSL). His research focuses on GNSS augmentation system design, analysis, and application. He received his M.S. and Ph.D. degrees in Aeronautics and Astronautics from Stanford University in 1999 and 2003, respectively.

ABSTRACT

Today, smart mobiles play an important role in our daily life. Most of these devices are equipped with a navigation function based on GNSS positioning. However, these devices may not work accurately in urban environments due to severe multipath interference and non-line of sight (NLOS) reception caused by nearby buildings. A promising approach for reducing the effect of multipath interference and NLOS reception is vector tracking (VT). VT is well-known for its robustness against poor signal-to-noise levels. However, its capability against multipath and NLOS has yet to be determined. The new combination of this paper is therefore to evaluate the performance of vector tracking in the presence of multipath and NLOS effects. A vector delay lock loop (VDLL) is used as the vector tracking technique. The noise tuning of the extended Kalman filter (EKF) in vector tracking is a key factor affecting its performance. Therefore, developed an adaptive noise tuning algorithm had been based on the measurement innovation. In order to evaluate vector tracking's performance, equivalent conventional tracking loops are used as a control.

GNSS signals were collected, while walking around in a challenging urban environment subject to multipath interference. The experimental results show that VT generates a more stable code numerical-controlled oscillator (NCO) frequency than CT does. This characteristic could reduce the impact of multipath interference which is reflected in a smaller position error using VT during most of run. To further test capability of VT against signal attenuation, this paper applies a signal cancellation method called direct signal cancellation algorithm to simulate the scenario of signal termination and NLOS reception. According to the simulation, VT provides not only robustness against signal termination but can also detect NLOS reception without any external aiding.

I. INTRODUCTION

Urban environments contain many flat surfaces that reflect the GNSS signals. Modern glass and metal buildings are particularly strong reflectors, while water enhances the reflectivity of most surfaces. Reception of these reflected signals results in significant positioning errors due to NLOS reception and multipath interference. These are often grouped together as "multipath". However, they are actually separate phenomena that produce very different ranging errors. NLOS reception occurs where the direct line-of-sight signal is blocked and the signal is received only via reflections. This results in a pseudo-range measurement error equal to the difference between path of reflected signal and the (blocked) direct path between satellite and receiver. This error is always positive and, although typically tens of metres, is

potentially unlimited. Multipath interference occurs where the signal is received through multiple paths between the satellite and user antenna. Both direct-line-of-sight and NLOS signals may be subject to multipath interference. The pseudo-range errors due to multipath interference can be positive or negative and depend on the design of the user antenna and receiver design [7].

As described in [6], many multipath mitigation techniques have mp significant effect on the errors caused by NLOS signal reception. Therefore, it is important to treat multipath and NLOS as separate phenomena. The objective of this paper is therefore to evaluate the performance of vector tracking under the scenario of multipath interference and NLOS reception. The detail of the algorithm of vector tracking is introduced in next section.

Recently, researchers have studied multipath and NLOS mitigation using consistency checking which may be augmented with external aiding such as receiver height from a database [1]. However, the aiding information might not be easily obtained by all GNSS receivers. This paper focuses on pedestrian positioning without external aiding. In this case, receiver-based multipath and NLOS mitigation would be a strong candidate. Traditionally, this involves applying different discriminator designs to mitigate multipath. These discriminator designs can reduce the pseudo-range multipath error provided that the receiver's precorrelation bandwidth is sufficient, which is not always the case for consumer receiver. However they also decrease the receiver's sensitivity and do not reduce NLOS at all. New approaches to multipath and NLOS mitigation are therefore needed. A promising approach for reducing the effect of multipath interference is vector tracking. A combined flowchart of GNSS receiver with both conventional tracking (CT) and vector tracking (VT) modes is shown in Figure 1.

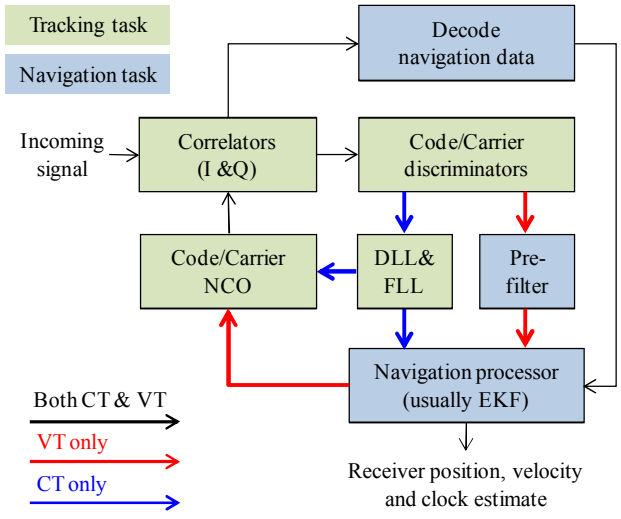

Figure 1: Flowchart of a GNSS receiver with conventional tracking loops and a vector tracking loop.

In the case of CT, the tracking and navigation processor are cascaded and independent of each other. As shown in Figure 1, the navigation processor does not feedback any information (including a navigation solution) to the conventional tracking loop. In fact, the code and carrier frequency are varied due to the relative motion between satellite and receiver. Thus, knowledge of the satellite's and receiver's velocities could be used to aid the receiver's tracking performance. However, CT tracks all channels individually and independently. The geometry of the satellite-user paths means that the measurements are never truly independent [2]. In comparison to the CT, VT replaces the delay lock loop (DLL) and sometimes the phase lock loop (PLL) with an extended Kalman filter (EKF) to track the GNSS signals, as shown in Figure 1 This VT EKF not only tracks the signals but also calculates the user positions. By combining the tracking and positioning tasks, VT can use the user motion determined from the stronger GNSS signals to predict the code phase and thus maintain tracking lock of the weaker signals. Thus, VT is typically more robust against signal interference and attenuation [3]. For example, the much improved performance of VT over conventional tracking in a large and heavy dense foliage forest has been demonstrated by a previous study [4]. VT also has the potential to mitigate the effects of multipath interference and NLOS reception. The objective of this paper is therefore to investigate the level of immunity against the effect of multipath interference generated by vector tracking.

The VT technique selected for this paper is the vector delay lock loop (VDLL) which replaces the individual DLLs but retains conventional FLLs to separates with the carrier phase of each signal. The alternative vector delay and frequency lock loop (VDFLL) also replaces the individual FLLS [7]. However, the simple VDLL is suitable for assessing the multipath mitigation ability of VT because multipath has a greater impact on the code than on the carrier. Here, an 8-state EKF with adaptive tuning is used to estimate the user position and maintain code tracking. The states estimated are user position, user velocity, receiver clock bias, and receiver clock drift. The EKF's adaptive tuning algorithm uses the variance of the measurement innovation to determine the assumed measurement noise covariance.

Even in the presence of multipath interference, the position error is often dominated by the tropospheric and ionospheric errors, particular for single-frequency receivers. To better observe the multipath effect, the International GNSS Service (IGS) exact ionospheric model and Saastamoinen troposheric delay model with UNB3 model are used to minimise the residual ionospheric delay and tropospheric delay, respectively. After applying these error models, multipath should be the main source of position error. In order to evaluate the multipath mitigation performance of the VT, the performance obtained from an equivalent conventional receiver is also required. The conventional receiver

utilizes an 8-state EKF for positioning with system and carrier measurement models identical to those of the VT EKF. The common parameters of the conventional and VT receivers, including the bandwidth of the FLL, the gain of FLL and the tuning parameters of EKF are all aligned.

Our previously developed Matlab-based GPS software-defined receiver [5] has been adopted as the research platform and self-developed VT algorithms implemented within it. The positioning and tracking performances of the CT and VT implementations are compared using a common set of intermediate frequency signals recorded at the Tzu-Chang campus of the National Cheng Kung University. A NovAtel SPAN-CPT, a professional-grade integrated INS/GPS system, was selected to provide the reference results. Moreover, this paper applies a direct signal cancellation algorithm to simulate the scenarios of signal blockage and NLOS reception.

Accordingly, this paper is organized as follow: Section II details the complete VDLL algorithm and the adaptive noise tuning algorithm used in this paper. The equivalent conventional tracking and error models applied in this paper are introduced in Section III and IV. Section V, describes the experiment setup and results. The simulation of direct signal outage and NLOS reception is described in Section VI. Finally, the concluding remarks and of this paper and proposed future work are presented in Section VII.

II. VECTOR TRACKING LOOP ALGORITHM

The vector tracking technique selected for this paper is the VDLL, which replaces the individual DLLs but retains conventional FLLs to track the carrier frequency from each signal. This is suitable for assessing the multipath mitigation ability of vector tracking because multipath has a greater impact on the code than on the carrier.

The architecture of the VDLL implemented in this paper is displayed in Figure 3. It is important to note that the vector tracking uses conventional tracking to facilitate its initialization. To initialize the vector tracking, the minimum requirement is that at least four signals from different satellites are tracked by conventional tracking. In other words, the code frequency, Doppler frequency, satellite ephemeris, and receiver position/velocity estimated by a conventional receiver are adopted to activate the vector tracking.

As shown in Figure 3, the calculation of code and carrier discriminator outputs is based on the correlation values of the channels, prompt, early, and late, in-phase and quadrature. In this paper, the selected frequency discriminator is *ATAN2* and the loop filter is a 2nd order loop filter [9] with 5Hz noise bandwidth. The code discriminator is an early minus late envelop discriminator with one chip spacing (early-late) [9]. The code discriminator outputs are fed into a non-coherent prefilter. The non-coherent prefilter calculates and smoothes the measurements for the following EKF [7]. Note that the Doppler measurement is not required to be smoothed by the non-coherent prefilter because it is smoothed in the 2nd order loop filter.

The measurements used in the EKF are delta pseudorange, $\Delta\rho^j$, and pseudorange rate, $\dot{\rho}^j$. The delta pseudorange here means the differences between true and predicted pseudorange. They are given by:

$$\begin{aligned} \Delta\rho^j \text{ (unit: meter)} &= \textit{code discri}^j \text{ (unit: chip)} \times \frac{c}{f_0} \\ \dot{\rho}^j \text{ (unit: } \frac{\text{meter}}{\text{sec}}\text{)} &= \textit{Doppler freq}^j \text{ (unit: Hz)} \times \frac{c}{f_{L1}} \end{aligned}, \quad (1)$$

where c is the speed of light, f_0 is the chipping rate (1.023 MHz for GPS C/A code), and f_{L1} is the L1 band carrier frequency (1575.42 MHz for GPS L1 signal). The EKF utilized in the VDLL not only tracks the code but also estimates the navigation solution. The state vector (**x**) of the EKF comprises the navigation solution error, and receiver clock error:

$$x = \begin{bmatrix} \Delta p_{xk} \\ \Delta p_{yk} \\ \Delta p_{zk} \\ \Delta v_{xk} \\ \Delta v_{yk} \\ \Delta v_{zk} \\ \Delta b_k \\ \Delta d_k \end{bmatrix} = \begin{bmatrix} \text{X-axis Position Error} \\ \text{Y-axis Position Error} \\ \text{Z-axis Position Error} \\ \text{X-axis Velocity Error} \\ \text{Y-axis Velocity Error} \\ \text{Z-axis Velocity Error} \\ \text{Clock Bias Error} \\ \text{Clock Drift Error} \end{bmatrix}. \quad (2)$$

The navigation error estimates are fed back to correct the navigation solution at each epoch would be clever. The position and velocity error states are resolved in and referenced at Cartesian earth-centred earth-fitted (ECEF) frame while the clock bias and drift are in units of meters and meters per second, respectively. The initial values of all states are zero. The EKF updates the error states using the incoming measurements from the non-coherent prefilter and FLL described previously and predicts the error states using a model of receiver dynamics. Finally, the predicted error states are applied to correct the navigation solution. The error states are then reset to zero for the next epoch of calculation. The detail algorithm of the EKF can be found in [7]. The system propagation of the EKF in this paper given by:

$$\hat{x}_k^- = \Phi_{k-1}\hat{x}_k^+, \quad (3)$$

where

$$\Phi = \begin{bmatrix} I_{3\times3} & \tau I_{3\times3} & 0_{3\times2} \\ 0_{3\times3} & I_{3\times3} & 0_{3\times2} \\ 0_{2\times3} & 0_{2\times3} & K \end{bmatrix}_{8\times8} \quad K = \begin{bmatrix} 1 & 1 \\ 0 & 1 \end{bmatrix},$$

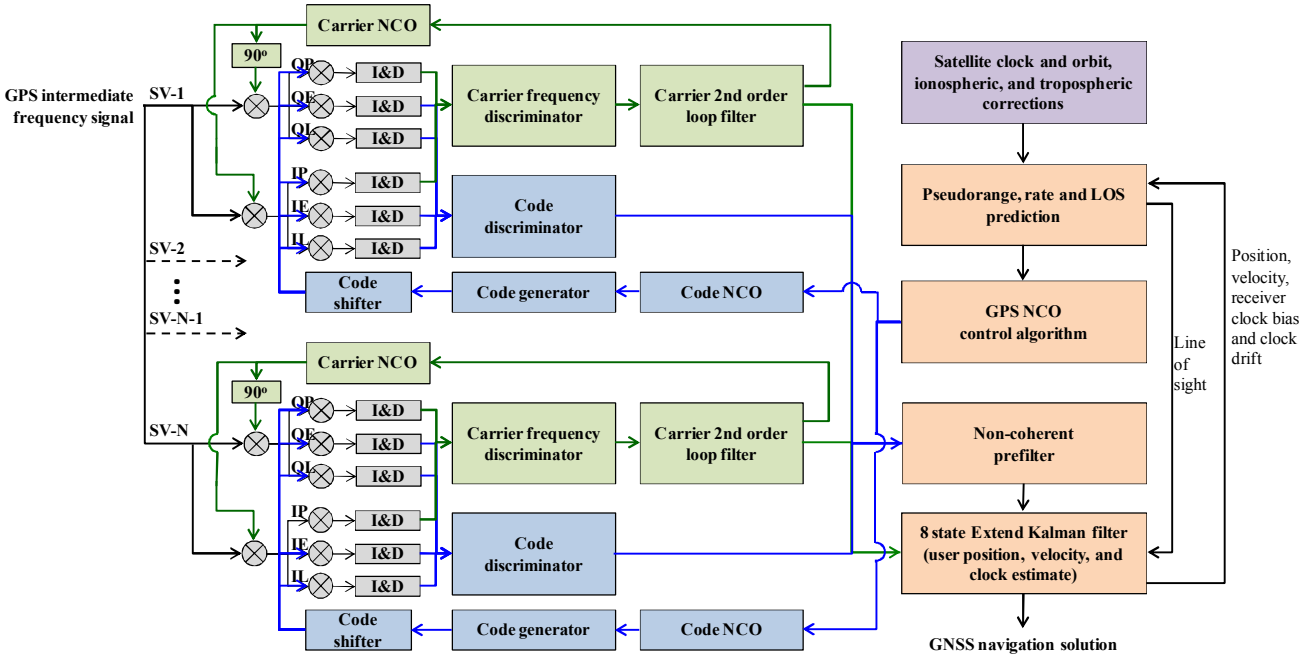

Figure 3: The detail architecture of the developed VDLL in this paper. I&D in the figure stands for integrate and dump.

τ is the integration interval (20 milliseconds in this paper), the subscript denotes the k^{th} epoch, superscript + denotes after measurement update, superscript – denotes after state propagation and before measurement update, and carat ˆ indicates result estimated by Kalman filter. The relation between the state vector and measurement vector is linearized by Taylor's expansion [7]. Thus,

$$\Delta\rho_k = H_k \Delta x_k \,, \tag{4}$$

where

$$\Delta\rho_k = \begin{bmatrix} \Delta\rho_k^1 \\ \Delta\rho_k^2 \\ \vdots \\ \Delta\rho_k^N \\ \Delta\dot{\rho}_k^1 \\ \Delta\dot{\rho}_k^2 \\ \vdots \\ \Delta\dot{\rho}_k^N \end{bmatrix} = \begin{bmatrix} \text{SV 1 delta Pseudorange} \\ \text{SV 2 delta Pseudorange} \\ \vdots \\ \text{SV N delta Pseudorange} \\ \text{SV1 Pseudorange-rate} \\ \text{SV2 Pseudorange-rate} \\ \vdots \\ \text{SV N Pseudorange-rate} \end{bmatrix}, \text{ and}$$

$$H = \begin{bmatrix} -u_x^1 & -u_y^1 & -u_z^1 & 0 & 0 & 0 & 1 & 0 \\ -u_x^2 & -u_y^2 & -u_z^2 & 0 & 0 & 0 & 1 & 0 \\ \vdots & \vdots & \vdots & \vdots & \vdots & \vdots & \vdots & \vdots \\ -u_x^n & -u_y^n & -u_z^n & 0 & 0 & 0 & 1 & 0 \\ 0 & 0 & 0 & -u_x^1 & -u_y^1 & -u_z^1 & 0 & 1 \\ 0 & 0 & 0 & -u_x^2 & -u_y^2 & -u_z^2 & 0 & 1 \\ \vdots & \vdots & \vdots & \vdots & \vdots & \vdots & \vdots & \vdots \\ 0 & 0 & 0 & -u_x^n & -u_y^n & -u_z^n & 0 & 1 \end{bmatrix}$$

where u indicates line of sight unit vector between satellite and receiver (user to satellite), and its superscript and subscript are j^{th} satellite and xyz dimension, respectively. The measurement vector is provided by non-coherent pre-filter and carrier loop filter as shown in (1). The linearized equation and system propagation equation are applied to calculate the measurement innovation in the updated stage of Kalman filter algorithm.

$$\delta z^- = \begin{bmatrix} \Delta\tilde{\rho}^1 \\ \Delta\tilde{\rho}^2 \\ \vdots \\ \Delta\tilde{\rho}^N \\ \tilde{\rho}^1 - \hat{\rho}^1 \\ \tilde{\rho}^2 - \hat{\rho}^2 \\ \vdots \\ \tilde{\rho}^N - \hat{\rho}^N \end{bmatrix}, \tag{5}$$

where δz^- denotes the measurement innovation, $\Delta\tilde{\rho}$ denotes the code measurement (as shown in (1)), $\tilde{\dot{\rho}}$ denotes the carrier measurement (as shown in (1)), and $\hat{\dot{\rho}}$ denotes the predicted carrier measurement. Then the state vector is updated by the measurement innovation and propagated by system dynamic model as describe in [7]. It is essential using the corrected navigation solution and clock offset estimate to generate the code NCO command and addressed in (6). This code NCO command is used to generate the replica code within the receiver.

$$\hat{f}^j_{co,NCOj,k+1} = f_0\left[1 - \frac{\left(\hat{\rho}^j_{R,k+1} - \hat{\rho}^j_{R,k}\right)}{c\tau}\right] \tag{6}$$

where f_0 is the code chipping rate, c is the speed of light, and $\hat{\rho}^j_{R,k}$ is the predicted pseudorange of the j^{th} satellite at the k^{th} epoch. The predicted pseudorange is calculated by:

$$\hat{\rho}^j_{R,k} = \sqrt{\left[\hat{r}^j_s - \hat{r}_j\right]^T\left[\hat{r}^j_s - \hat{r}_a\right]} + \delta\hat{\rho}^j_{sv,c} + \delta\hat{\rho}^j_T + \delta\hat{\rho}^j_I - \hat{b}_k \text{ , (7)}$$

where $\hat{r}^j_s$ is the j^{th} satellite position, $\hat{r}_a$ is the receiver position, $\delta\hat{\rho}^j_{sv,c}$ is the satellite clock correction, $\delta\hat{\rho}^j_T$ and $\delta\hat{\rho}^j_I$ are the tropospheric and ionospheric error estimates, respectively. The tropospheric and ionospheric models applied in this paper will be discussed in Section V. By giving feedback of the code frequencies to the code NCO, all channels are processed jointly. Because more information is used to generate the NCO commands, vector tracking enjoys a better performance in terms of receiver sensitivity.

The tuning of the EKF is a key factor of its performance. The most common noise calibration method is to adjust the measurement noise covariance matrix (R), the process noise covariance matrix (Q) and the state estimation error covariance matrix (P) by using empirical data. In general, however, the optimum tuning of the noise covariance matrices will vary according to the environments. This paper therefore develops an adaptive tuning algorithm for the developed VDLL. The P matrix is initialised with the initial uncertainty of the navigation solution and clock errors. The main sources of process noise are acceleration and deceleration of the user motion and the random walk of the receiver clock. Thus, the process noise covariance Q can be divided into user dynamic noise and receiver clock noise.

$$Q = \begin{bmatrix} K_{dynamic} & 0_{6\times 2} \\ 0_{2\times 6} & K_{clock} \end{bmatrix}, \tag{8}$$

where,

$$K_{dynamic} = \begin{bmatrix} \tau^3/3 & 0 & 0 & \tau^2/2 & 0 & 0 \\ 0 & \tau^3/3 & 0 & 0 & \tau^2/2 & 0 \\ 0 & 0 & \tau^3/3 & 0 & 0 & \tau^2/2 \\ \tau^2/2 & 0 & 0 & \tau & 0 & 0 \\ 0 & \tau^2/2 & 0 & 0 & \tau & 0 \\ 0 & 0 & \tau^2/2 & 0 & 0 & \tau \end{bmatrix} \cdot S_v \text{ ,}$$

$$K_{clock} = \begin{bmatrix} S_{c\phi}\tau + \frac{1}{3}S_{cf}\tau^3 & \frac{1}{2}S_{cf}\tau^2 \\ \frac{1}{2}S_{cf}\tau^2 & S_{cf}\tau \end{bmatrix}, \begin{cases} S_{c\phi} = c^2 \cdot \dfrac{h_0}{2} \\ S_{cf} = c^2 \cdot 2\pi^2 \cdot h_{-2} \end{cases},$$

where τ is the update interval, S_v is the user velocity noise power spectrum density (PSD), $S_{c\varphi}$ is the oscillator phase noise PSD, and S_{cf} is the oscillator frequency noise PSD. The user velocity PSD is determined by the expected user dynamics. In this paper, S_v is 1 m^2/s^3 for the dynamic scenario. The front-end selected here is an IP-Solution J-type front-end with temperature compensated crystal oscillator (TCXO.) According to [10], the coefficients of the TCXO are:

$$\begin{aligned} h_0 &= 2\times 10^{-19} \\ h_{-2} &= 2\times 10^{-20} \end{aligned}. \tag{9}$$

The measurement noise covariance matrix is updated adaptively. The off-diagonal terms of the adaptive R are zero due to the low cross-correlation characteristic between each channel. This paper employs the variance of the measurement innovation (5) as the main diagonal terms of R. Small measurement innovation values mean that the incoming measurements are similar to the predicted measurements ($H_k\hat{x}_k^-$). This might imply either that the quality of the measurements is high or that the EKF is capable of predicting the measurement changes. Either of these cases indicates that a small measurement innovation value is worth high confidence. Conversely, a large measurement innovation value implies low confidence. In summary, the adaptive measurement noise covariance is shown as bellow:

$$R = diag\begin{bmatrix} f_p \cdot E(\delta z^-_{\rho,1}) \\ \vdots \\ f_p \cdot E(\delta z^-_{\rho,N}) \\ f_p \cdot E(\delta z^-_{\dot{\rho},1}) \\ \vdots \\ f_p \cdot E(\delta z^-_{\dot{\rho},N}) \end{bmatrix}^T, \tag{10}$$

where f_p is a compensated factor of adjusts the measurement noise covariance to account for the time-

correlatec measurement noise. In the developed VDLL, the carrier noise bandwidth is 5Hz which is 10 times faster than the update rate of the EKF. A compensated factor, 10, is suggested due to the empirical experience. The time window applied to calculate the measurement innovation variance is 20 seconds in this paper. These measurement noises are also restricted by with a given maximum and minimum threshold. The maximum and minimum thresholds of the code measurement are 5000 and 0.01 meter^2, and 50 and 0.01 meter^2/second^2 for carrier measurement. The thresholds for vector and conventional tracking are identical.

III. EQUIVALENT CONVENTIONAL RECEIVER

This paper aims to discover benefits of vector tracking. It assigns an equivalent conventional receiver as a control group in performance evaluations. Based on different applications, positioning solutions could be estimated by a least-squares algorithm or a Kalman filter. In the case of a least-squares algorithm, it is unfair to compare the performance between vector and conventional receivers because any improvements exhibited by vector tracking might be due to Kalman filter. Unlike a least-squares algorithm, Kalman filter uses knowledge of the user dynamics and noise properties. Here, the EKF used with the conventional receiver has identical system and carrier measurement model to the vector tracking EKF. The states of the EKF in the equivalent conventional receiver are also receiver position, velocity and clock bias and drift. The noise tuning of this EKF is identical with the one in vector tracking. In comparison to the developed VDLL, there are two major differences between the equivalent conventional receiver and the vector one. The first is the calculation of measurement, more specifically the formation of delta pseudorange. Vector tracking uses code discriminator's output to obtain the difference between true and predicted pseudorange. This delta pseudorange is used as measurements for the EKF of vector tracking. In conventional receivers, the pseudorange is estimated by the speed of light multiplying time differences. The calculation is as below:

$$\rho^j = c\left(TOT^j - TOA\right), \qquad (11)$$

where ρ^j is the pseudorange of the j^{th} satellite, *TOT* is the time of transmit from a satellite, and *TOA* is the time of arrival in a conventional receiver. In conventional tracking, its delta pseudorange is calculated by the measured pseudorange (11) minus the predicted pseudorange (the range between satellite's position and previous receiver's position solution plus the estimated clock offset). The second difference is that the conventional receiver utilized a 2nd order loop filter to track the code of each channel. This implies that the equivalent conventional receiver tracks all channels independently. Note that conventional tracking does not return code or carrier frequencies from the EKF to the NCOs. These two differences contribute the difference between conventional and vector tracking. Thus, it is reliable to adopt an equivalent conventional receiver as a control to compare the performance of the developed VDLL against.

IV. CORRECTION MODELS

According to the GPS error budget [7], as shown in Table 1, the position error of single-frequency receivers is often dominated by the tropospheric and ionospheric errors even in the presence of multipath interference. The medium-range multipath error represents 0-20 meter range model.

Table 1: Standard deviation of range error component [7]

Residual of error sources	*Error standard deviation (m)*
Satellite clock and ephemeris errors	0.9
Ionosphere error[1]	0.8
Troposphere error[2]	0.2
Medium-range multipath error	0.94

1: Assuming IGS exact ionospheric model
2: Assuming latitude- and season-dependent model

The tropospheric error residual is 0.2 meter when applying a latitude- and season-dependent model. This paper utilizes a combination of Saastamoinen zenith delay model and Black & Eisner mapping function to minimise the troposheric error. It selects a UNB3 model to provide parameters for the tropospheric model mentioned above. The detail of these algorithms can be found in [11-12]. A general ionospheric correction model for a single-frequency is the Klobuchar model. However, it can only model about 50% of the ionospheric error. As a result, the ionospheric error residual in Table 1 is 0.9 meter. In order to more easily observe the multipath effect, this paper utilizes the international GPS service (IGS) exact ionospheric model to further reduce the error. The IGS publishes a global total electron content (TEC) map to provide users around the world to estimate the ionospheric delay. To apply the IGS model, the users have to interpolate their own TECs and calculate the ionospheric delay from them [13]. The IGS exact ionospheric model is proven to reduce at least 80 percent of the ionospheric error [13]. After applying these error models, multipath should be the main source of position error.

V. EXPERIMENTAL SETUP AND RESULTS

In previous work, a GPS L1 software defined receiver (SDR) was developed [5]. This SDR has the flexibility to implement different tracking and navigation algorithms. The IP-solutions J-Type front-end, which is TCXO based, was used to collect data. The precorrelation bandwidth of the front-end is 4MHz. The IF and sampling frequency are 4.123968 MHz and 16.367667 MHz, respectively. A NovAtel active airborne 4G1215A-XT-1 antenna was selected because it is usually used in no multipath scenarios (i.e., it does not mitigate multipath). A NovAtel

SPANCPT, a sophisticated GPS/INS integrated receiver, was chosen as the reference for the experiment. The NovAtel SPANCPT and the IP-solutions front-end shared the antenna via a GPS Networking antenna splitter. The overall architecture of experimental equipment is shown in Figure 4.

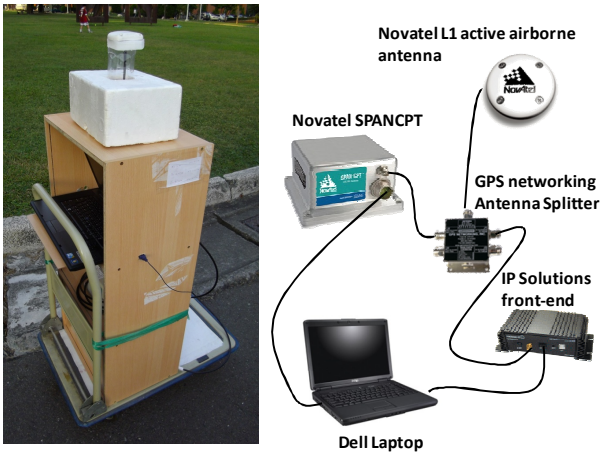

Figure 4: Architecture of the experimental equipment used in this paper.

Tzu-Chang Campus of NCKU was selected as the experimental area due to its high potential for multipath interference. A 15-story building is expected to block and reflects GNSS signals. This paper mainly focuses on the application of urban pedestrian navigation. As a result, it targets the horizontal positioning performance obtained during the dynamic experiment. The experiment was conducted on February 23, 2012, at 08:45 AM (UTC). The dynamic scenario is shown in Figure 5 where the black line is the position solutions calculated by NovAtel SPANCPT. The calculated C/N_0 of the NovAtel receiver is displayed in Figure 6. There are six trackable satellites applied in the dynamic experiment. All of the satellites signals fluctuate throughout the experiment the since dense foliage and buildings that surrounded the square route attenuate the signals. In general, the reference solution is smooth and accurate, achieving a horizontal accuracy of 0.02 meter [14]. Noticeably, there is an outage of the NovAtel receiver during section A of Figure 5.

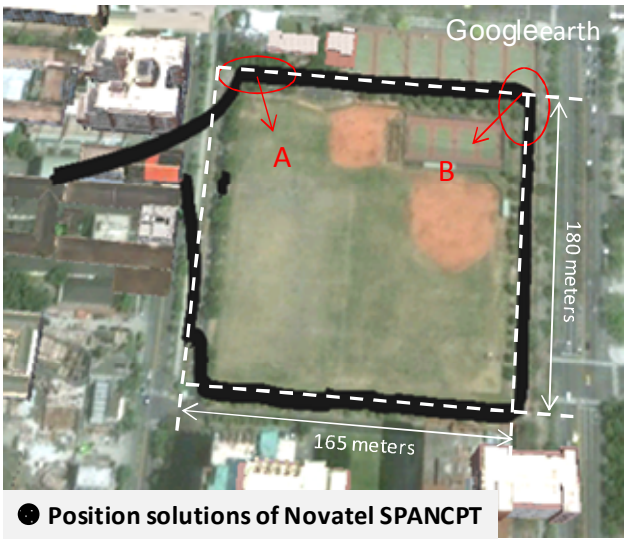

Figure 5: Environment of the dynamic experiment, and trajectory of NovAtel SPANCPT.

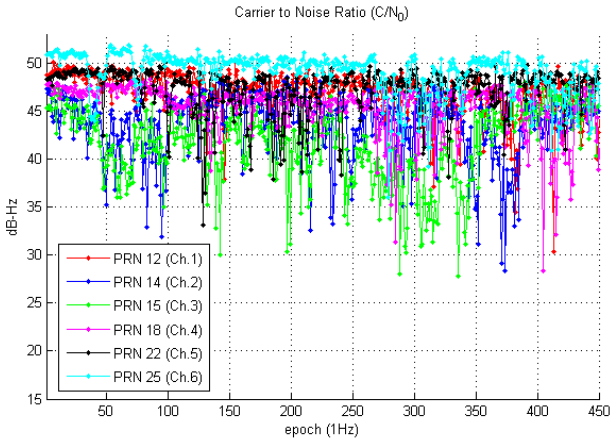

Figure 6: C/N_0 values calculated by NovAtel SPANCPT in the dynamic experiment

This outage is caused by the nearby building obstructions as shown in Figure 7. Two of the six channels, the second and the third channel, are affected by the buildings.

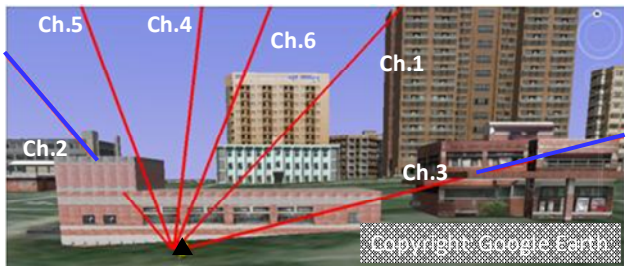

Figure 7: Environment of section A of the dynamic experiment.

It is indicated by indicates the significant C/N_0 oscillations of the second and the third channel between the 300th and 400th epochs (the period corresponding section A) in Figure 6. Thus, it is supposed that these signals in section A are affected by multipath effects, NLOS reception, and diffraction. Section B ranges between 200th epoch and 250th epoch of Figure 6 and is

also influenced by signal attenuations. Figure 8 shows the VT's positioning results and the reference position solution. According to the figure, VT is capable of maintaining the performance during the section B of Figure 5 (where multipath interference is present). However, there is an outage from the NovAtel receiver observed in Figure 8. This paper therefore only considers the reference position solutions before the outage occur.

The positioning errors of CT and VT are illustrated in Figure 9. The positioning error is calculated by subtracting the solutions provided by NovAtel SPANCPT from the positioning results of CT or VT. VT is activated only if the CT has stable performance. In the first 1000 epochs, the error of VT is larger than that of CT because of its noise variance calibrating process. As previously mentioned, VT requires an amount of time to optimize its performance through self-calibration. After 1000 epochs, VT works better than CT does most of the time. The 2D RMSEs of CT and VT are 2.60 and 1.51 meters, respectively. It is important to note that this paper applied the Saastamoinen model and IGS exact ionospheric model to minimize the tropospheric and ionospheric delays. As a result, the multipath interference is assumed to be the dominant error in this experiment. The results in Figure 9 indicate that VT's overall positioning performance is better than CT's. This improvement implies that VT is able to reduce the effects of multipath interference. In order to further investigate the immunity against multipath interference generated by VT, the paper continues to focus on sections A and B of Figure 5. As discussed above, there are considered to be the locations with the most severe multipath effects. Now the results are shown in Figure 10 and Figure 11.

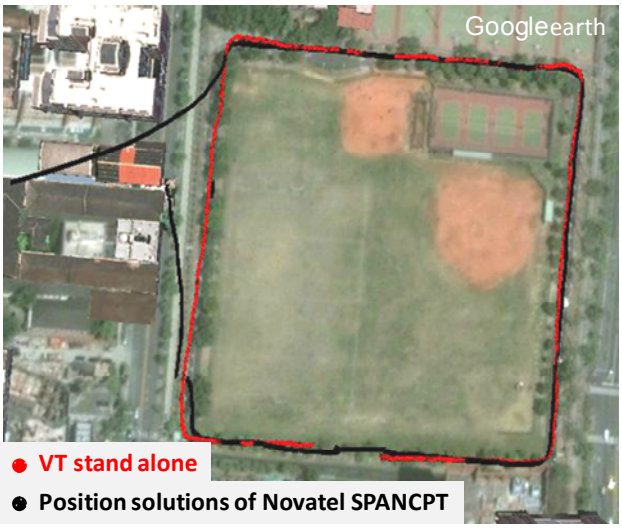

Figure 8: Positioning results of VT in Google Earth.

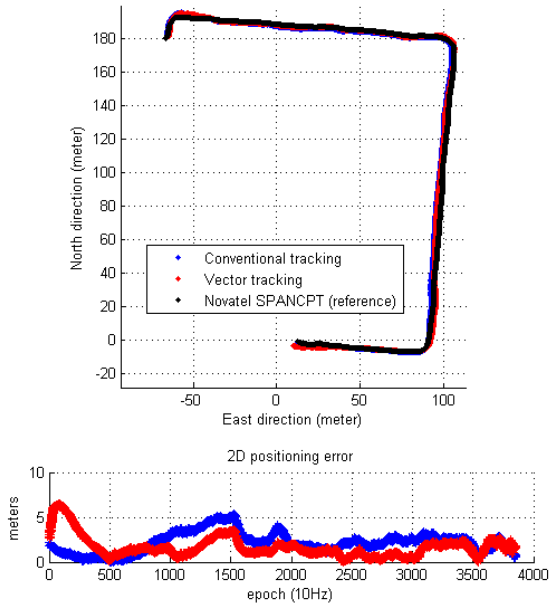

Figure 9: Positioning errors of CT and VT in the dynamic experiment.

As can be seen in Figures 10 and 11, VT and CT exhibit similar performance in both sections. However, the VT's positioning error is lower than that of CT for most of the time. The 2D root mean square errors (RMSEs) of CT and VT in section A are 2.02 and 1.93 meters, respectively. The 2D RMSEs of CT and VT in section B are 1.68 and 1.42 meters, respectively. Thus, the vector tracking only provides a few centimeters of improvement in the positioning solution in these two sections. An analysis of the assumed measurement noise covariance (R) was conducted to investigate VT's benefits, which is shown in Figure 12. The measurement noise covariance is estimated by the adaptive tuning algorithm described in Section II. The measurement innovation given by (5) is used as the basis for calculating the assumed measurement noise covariance.

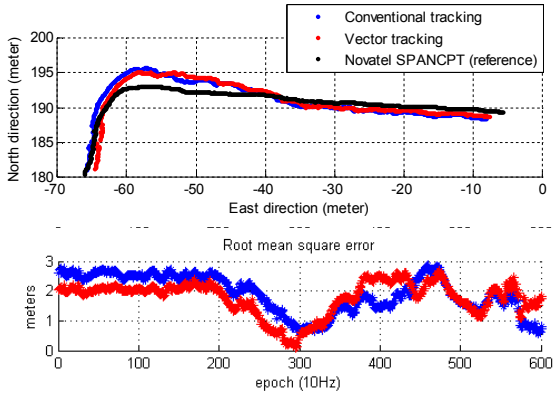

Figure 10: Positioning results of the three methods in section A of the dynamic experiment.

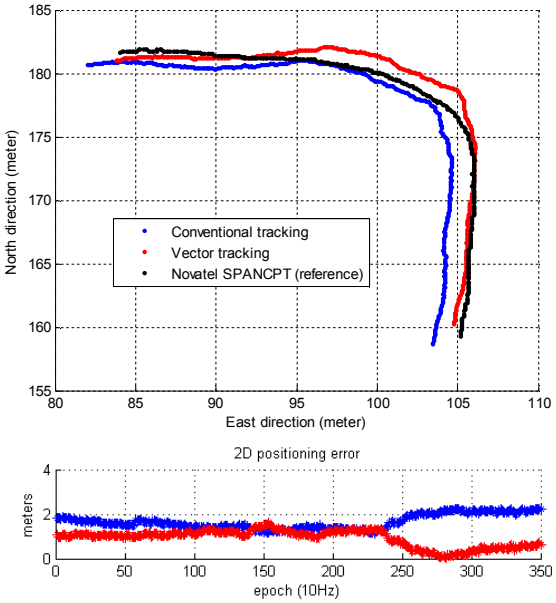

Figure 11: Positioning results of the three methods in section B of the dynamic experiment.

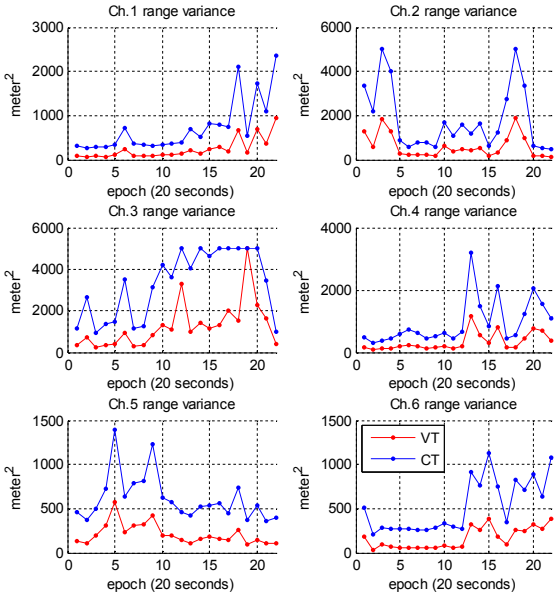

Figure 12: Measurement noise covariance assumed in the VT and CT EKFs in the dynamic experiment.

Figure 12 demonstrates that the measurement noise variance estimated by VT is smaller than by that estimated CT for most of the time. As discussed in Section II, smaller noise variances may indicate either better signal quality or a better estimation of the changes. Therefore, VT can predict signal changes more accurately than CT. It is interesting to analyze sections A and B of Figure 5 in terms of measurement noise. The period of section A is between the 17th and 20th epochs in Figure 12. The measurement noise variances estimated by VT are much smaller than those estimated by CT in the 1st, 4th, 5th and 6th channels. Smaller noise variances indicate a better estimate of signal changes (usually are signals with higher quality). As shown in Figure 6, these channels typically have a higher C/N_0than others. In these cases, VT reports higher confidences on these healthier channels. For the 2nd and 3rd channels, the noise covariances estimated by VT and CT are similar. In other words, VT reports less confidence in the 2nd and 3rd channel in comparison with the other channels. This higher noise variance may imply the signal is attenuated by multipath effects and interferences. Figure 7 demonstrates the signal blockage in the 2nd and 3rd channels. Thus, VT can help receiver to distinguish whether the signal is affected by multipath effect or not. The period of section B is between the 11th to 13th epochs in Figure 12. Here, VT detects the signal attenuation in the 3rd channel while reporting less confidence compared with other channels.

In order to determine the mechanism by which VT given better performance, the tracking results of the third channel is analysed in Figure 13. The discussion mainly focuses on estimated the code frequency. As explained in Section III, the difference in the estimation of code frequency is one of the major differences between the VDLL developed here and the equivalent conventional tracking loop.

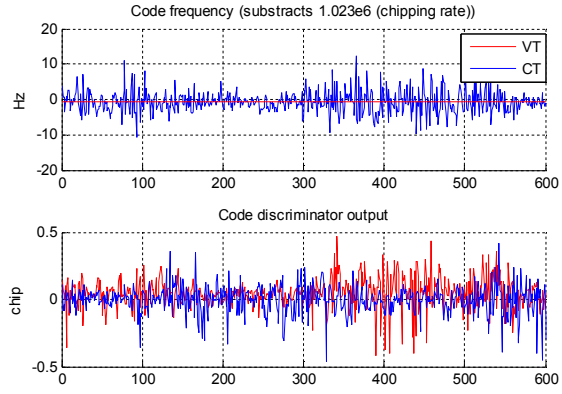

Figure 13: Tracking results of the 3rd channel in section A of Figure 5.

In Figure 13, even through the VT's code discriminator outputs are noisy in section A, the code frequency estimated by VT is more stable than that estimated by CT. Unlike CT, VT calculates the code frequency not only from the incoming measurements but also using the system propagation model. In the case of section A (where multipath interference is present), VT exhibits less confidence in the calculation measurements because the code frequency mainly is based on the system propagation model. Overall, this demonstrates the resistance against

multipath interference exhibited by VT in this experiment using real signals.

VI. SCENARIOS OF SIGNAL OUTAGES AND NLOS RECEPTIONS

This paper also aims to investigate the VT's performance in terms of signal blockage and NLOS reception. However, datasets containing these biased signals are not readily available. As a result, this paper applied an algorithm called direct signal cancellation [15] to cancel the presence of the signal in one channel and thus the effect of investigate signal blockage. The initial objective of this signal cancellation technique was to enhance the receiver sensitivity by eliminating the multiple access interference between strong signal and weak signal. The idea of direct signal cancellation is to generate a perfect signal replica (one satellite only) based on the tracking results. Then, the collected IF signal is subtracted directly with the generated signal replica. As a result, the newly generated IF signal will no longer contain the signal from the particular satellite. The simulation of signal blockage is based on the real signal discussed in the previous section. This paper cancels the signal in the 6th channel of the collected IF signal due to its relatively stable and high signal to noise ratio. The duration of the signal blockage is ten seconds. Figure 14 shows the positioning results of VT and CT during the period of the simulated signal termination.

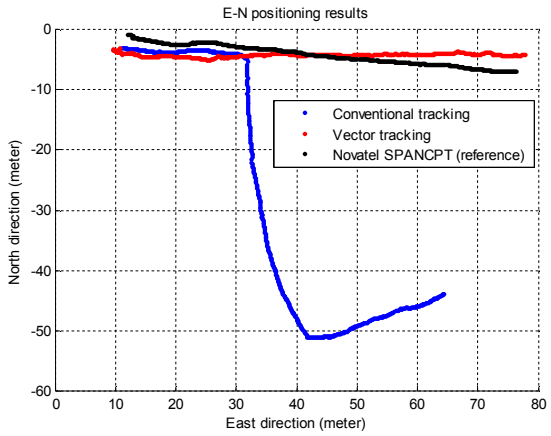

Figure 14: Positioning results of the simulated scenario of signal blockage.

Obviously, VT maintains stable positioning performance during the period of signal termination in Figure 14. In contrast, the signal blockage affects the CT solution, which is also show in Figure 14. Figure 15 shows the tracking performance of VT and CT. The signal termination is between 190th and 290th epochs in Figure 15. The middle of Figure 15 is the code discriminator output. The discriminator outputs of both VT and CT are very noisy. These noisy outputs from CT's code discriminator affect its ability to maintain code lock. As a result, CT can't maintain the code frequency lock which induces a false carrier frequency lock. In comparison to CT, VT has greater robustness against signal anomalies. Although the VT's code discriminator also has a noisy output, its estimate of both the code and carrier frequencies is still stable during the signal termination.

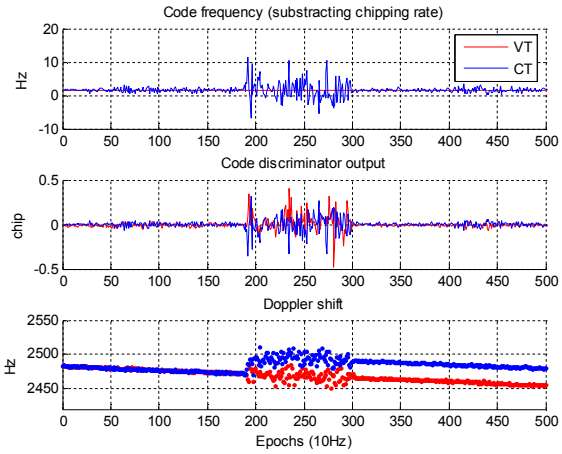

Figure 15: Tracking results of 6th channel in the simulated scenario of signal blockage.

NLOS signals are received only via reflected surfaces and can contribute large ranging errors. If these signals were identified and excluded, the positioning accuracy could be improved. In order to test the VT's performance in the presence of NLOS reception, the signal in the 6th channel and a reflected signal from the same satellite added in its place. The reflected signal is –6dB weaker than the direct line of sight (LOS) signal and delayed by 0.9 chips relative to the direct path. The positioning results using both tracking techniques are shown in Figure 16.

Unsurprisingly, both techniques are misled by the effects of NLOS reception. However, the result shows that VT has an opportunity to detect the NLOS reception. In Figure 16, VT positioning solution is received jumps dramatically as soon as the NLOS signal. The trend can be observed from tracking data shown in Figure 17. The constitute plot from top to bottom are the estimation of code frequency, the code discriminator output, VT's correlation values in early, prompt, and late channels, and CT's correlations value in the early, prompt, andlate channels.

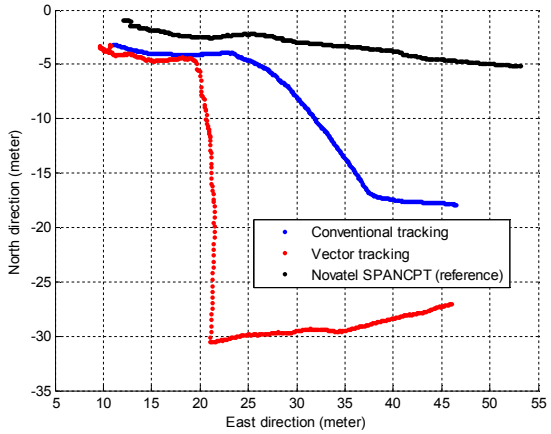

Figure 16: Positioning results of the simulated scenario of NLOS reception.

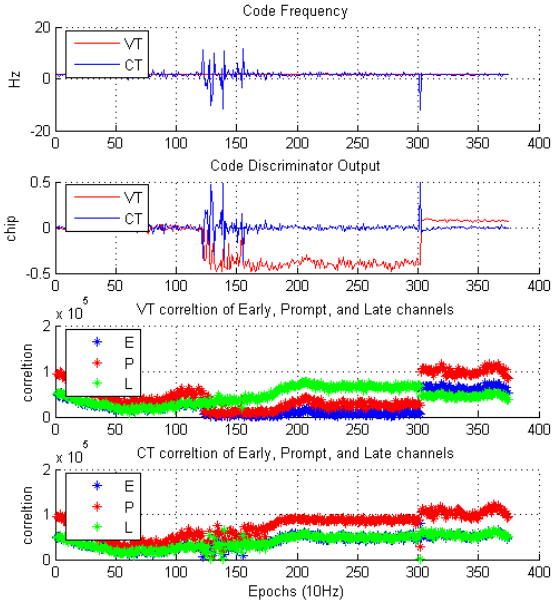

Figure 17: Tracking results of the 6th channel in the simulated scenario of NLOS reception.

The period of NLOS reception is between the 122th to 302th epochs. Looking at CT's code discriminator output, anomalies only occur at the beginning and end of the period of NLOS reception. In the bottom part of Figure 17, CT's correlation value in the prompt channel is the highest among the three during the period of NLOS reception. Because of this, it is difficult for CT to detect the effect of NLOS. On the other hand, VT's code discriminator output keeps discovering a code delay in the incoming signal during the period of NLOS reception. Furthermore, VT's highest correlation value is found in the late channel. This phenomenon implies that it could be a reflected signal received during the period of NLOS reception. Both VT's code discriminator output (second row of Figure 17) and correlation value (bottom of Figure 17) report that the channel is affected by a reflected signal. As mentioned before, VT estimates the change of signal not only from the incoming measurements but also via the system propagation of the state estimates. In general, the changes in signal parameters, including code frequency, phase, etc. should be smooth. VT achieves smooth estimates of the signal parameters using its system propagation model. Thus, VT is capable of detecting signal anomalies through comparing the predicted and incoming measurements. In the case of NLOS reception as shown in Figure 17, VT takes advantage of the state propagation model to estimate a stable code frequency regardless of the period of interference. Based on this stable code frequency, VT has the potential to detect the NLOS reception.

VII. CONCLUSIONS AND FUTURE WORK

This paper presents the first research which examines the resistance against multipath interference and NLOS reception exhibited by vector tracking. Real IF signals under dynamic condition were recorded where the signal is affected by multipath interference. According to the experiment results, vector tracking is shown to detect multipath interference through the increased variance of the measurement noise. In a serious severed multipath-affected area (such as Sections A and B in the experiment), a vector tracking loop outperforms the equivalent conventional tracking loop in terms of the accuracy of the position solution. In comparison to conventional tracking, vector tracking is able to generate a stable code frequency even in the presence of severe multipath interference.

A direct signal cancellation algorithm was used to simulate scenarios of NLOS reception and signal termination. In the simulation, vector tracking demonstrates robustness against signal outages. In the case of NLOS reception, the positioning results of both conventional and vector tracking are affected by the NLOS signal. However, vector tracking does present the opportunity to detect NLOS reception from the correlator output. Using the code discriminator output, vector tracking can detect the code phase offset caused by a NLOS signal.

The following future work is proposed. First, a simulation of different NLOS signals (in terms of reflected range, signal amplitude, etc.) will be conducted in the near future. Second, the authors will develop techniques for detections NLOS reception in a vector tracking loop.

ACKNOWLEDGMENTS

Li-Ta Hsu would like to thank Professor Marek Ziebart who provided him with the opportunity to study in Space Geodesy and Navigation Laboratory (SGNL) at University College London (UCL). The authors also thank Dr. Ziyi Jiang, Christopher Atkins, Santosh Bhattarai, John A. Momoh for providing thoughtful comments.

Finally, the first author acknowledges the Graduate Student Study Abroad Program (GSSAP) funded by National Science Council of Taiwan which provided the financial support for the academic visit to University College London. The GNSS research at Communication and Navigation Systems Laboratory in National Cheng Kung University is supported by National Science Council of Taiwan under project grant NSC 101-2628-E-006-013-MY3.

REFRERENCES

[1] Jiang, Z. and Groves, P.D., "GNSS NLOS and Multipath Error Mitigation using Advanced Multi-Constellation Consistency Checking with Height Aiding," *Proceedings of the 25th International Technical Meeting of The Satellite Division of the Institute of Navigation (ION GNSS 2012),* Nashville, TN, September 2012.

[2] Spilker, J.J., "Fundamentals of Signal Tracking Theory," in *Global Positioning System: Theory and Application Volume 1*, *Chapter 7*, B.W. Parkinson Ed., American Institute of Aeronautics and Astronautics, Washington DC, 1996.

[3] Lashley, M., Bevly, D.M., Hung, J.Y., "A Valid Comparison of Vector and Scalar Tracking Loops," *Proceedings of IEEE/ION PLANS 2010*, Indian Wells, CA, May 2010, pp. 464-474.

[4] Lashley, M., Bevly, D.M., "Comparison in the Performance of the Vector Delay/Frequency Lock Loop and Equivalent Scalar Tracking Loops in Dense Foliage and Urban Canyon," *Proceedings of the 24th International Technical Meeting of The Satellite Division of the Institute of Navigation (ION GNSS 2011)*, Portland, OR, September 2011, pp. 1786-1803.

[5] Hsu, L.T., Sun, C. C., Jan, S. S., "Comparison of Acquisition and Tracking Methods for Software Receiver," *Proceedings of 4th Asian Space Conference 2008*, Taipei, Taiwan, October, 2008.

[6] Groves, P.D., Jiang, Z., Wang, L., Ziebart, M.K., "Intelligent Urban Positioning using Multi-Constellation GNSS with 3D Mapping and NLOS Signal Detection," *Proceedings of the 25th International Technical Meeting of The Satellite Division of the Institute of Navigation (ION GNSS 2012)*, Nashville, TN, September 2012

[7] Groves, P.D., "Principles of GNSS, Inertial and Multi Sensor Integrated Navigation Systems", 2nd edition, Artech House, 2013.

[8] Bahrami, M., and M. Ziebart, "Instantaneous Doppler-Aided RTK Positioning with Single-Frequency Receivers," *Proc. IEEE/ION PLANS 2010*, Indian Wells, CA, May 2010, pp. 70-78.

[9] Ward, P. W., Betz, J. W., and Hegarty, C. J., "Satellite Signal Acquisition, Tracking, and Data Demodulation," in *Understanding GPS: Principles and Application, Chapter 5,* Kaplan E. D., Hegarty, C. J., Ed., *Artech House Publishers*, Norwood, MA, 2006.

[10] Brown, R. G., Hwang, P. Y. C., "Introduction to Random Signals and Applied Kalman Filtering," 3rd edition, *Wiley*, 1996.

[11] Saastamoinen, J., "Contributions to the theory of atmospheric refraction", In three parts: *Bulletin Géodésique*, No. 105, pp. 270-298; No. 106, pp. 383- 397; No. 107, pp. 13-34, 1973

[12] LaMance, J., Collins, P., Langley, R., "Limiting Factors in Tropospheric Propagation Delay Error Modelling for GPS Airborne Navigation," *Proceedings of the 52nd Annual Meeting of The Institute of Navigation*, Cambridge, MA, June 1996, pp. 519-528.

[13] Hernández-Pajares, M., Juan, J.M., Sanz, J., Orus, R., Garcia-Rigo, A., Feltens, J., Komjathy, A., Schaer, S.C., Krankowski, A., " The IGS VTEC maps: a reliable source of ionospheric information since 1998, " *Journal of Geodesy*, vol. 83, issue 3-4, Mar. 2009, pp. 263-275.

[14] NovAtel SPAN-CPT GPS/INS receiver product sheet,http://www.novatel.com/assets/Documents/Papers/SPAN-CPT.pdf. Last retrieved 17th Jan 2013.

[15] Hsu, L.T., Jan, S. S., Sun, C. C., Lin, Y. C., "A New Algorithm for the Signal Cancellation of GIOVE-A L1B & GPS L1 Signal," *Proceedings of International Symposium on GPS/GNSS 2007*, Persada Johor, Malaysia, November 2007.